



Numerical Modeling of Interactions between Solitary Waves and Floating Breakwaters

M. Tabatabaei Malazi^{1†}, A. S. Dalkilic² and S. Wongwises^{3,4}

¹ Department of Mechanical Engineering, Faculty of Engineering, Istanbul Aydin University, Istanbul 34295, Turkey

² Department of Mechanical Engineering, Faculty of Mechanical Engineering, Yildiz Technical University, Istanbul 34349, Turkey

³ Department of Mechanical Engineering, Faculty of Engineering, King Mongkut's University of Technology Thonburi, Bangkok 10140, Thailand

⁴ National Science and Technology Development Agency (NSTDA), Pathum Thani 12120, Thailand

†Corresponding Author Email: mahditabatabaei@aydin.edu.tr

(Received March 11, 2022; accepted June 28, 2022)

ABSTRACT

In the current numerical work, a 2D wave tank has been planned to explain the shared impacts among three different solitary waves and three different floating breakwaters by applying Reynolds-Averaged Navier-Stokes models and the volume of fluid method. Three dissimilar floating breakwaters (i.e., square breakwater, circular breakwater, and modified breakwater) were chosen. A total of eighteen cases were investigated, including three different floating breakwaters, a solitary wave (SW) with three different wave heights, and two different densities of floating breakwaters. We achieved the production of a solitary wave by moving a wave paddle (WP) and the motion of floating breakwater in two various directions by applying two different codes as user-defined functions. The dynamic mesh technique has been employed for re-forming mesh during the motion of the wave paddle and the floating breakwater. The numerical calculations have been confirmed by some numerical, analytical, and experimental case studies. First, the generation of a SW using the WP movement and the free motion of a heaving round cylinder on the free surface of motionless water were modeled and validated. Additionally, the effects of various parameters, including floating breakwater shape, floating breakwater density, and solitary wave height, on the hydrodynamic performances of the floating breakwater, the floating breakwater's motions, and the free-surface elevation were considered under various conditions.

Keywords: Floating breakwater; Wave-structure interaction; Solitary wave; CFD; VOF.

NOMENCLATURE

2-D	two-dimensional	P	pressure
CFL	Courant-Friedrichs-Lewy	PF	Positive Force
G_b	turbulent kinetic energy generation depending on buoyancy	RANS	Reynolds-Averaged Navier-Stokes
G_k	generation of turbulent KE	R_ε	term in the ε equation
F_D	drag force	S_ε	user-defined source term
F_L	lift force	SW	Solitary Wave
F_x	force in x-direction	t	time
F_y	force in the y-direction	u	velocity
H	solitary wave height	UDF	User-Define-Function
h	water depth	VOF	Volume of Fluid
k	turbulent kinetic energy	Y_M	fluctuating dilatation involvement
WP	Wave Paddle	ρ	density
NF	Negative Force	μ	dynamic viscosity
NWT	Numerical Wave Tank	Δx	cell size in x-direction
		Δy	cell size in y-direction
		Δt	time step
		η	free surface displacement
		ε	rate of dissipation

1. INTRODUCTION

Floating breakwaters are frequently applied to guard offshore constructions, such as offshore wind turbines, offshore petroleum wells, and ports, from waves. Investigations of the wave–floating breakwaters interaction have various advantages in controlling waves, lowering construction costs, and capturing energy from waves. Wave energy is among the up-and-coming renewable resources, and it has several advantages. For instance, it is environmentally friendly and economical; thus, floating breakwaters can be used as wave energy converters. Accordingly, much-related research recently has been carried out. Lin (2007) investigated a 2D constant-grid equation for the evaluation of free-surface flow under varying conditions. He solved some important fluid-structure interaction problems, such as the production of a SW by moving a WP, water outlet, and water influence. The outcomes illustrated that the novel 2D study may simulate multifaceted fluid-structure interaction difficulties with sufficient precision. Lin (2006) used a multiple-layer σ -coordinate study for wave–structure interface problem analysis. He represented free surface elevation during the SW’s mutual effect with a rectangular impediment at three different submergence depths. Wu *et al.* (2016) practically and computationally researched SW generation under different conditions. They generated a SW by moving a WP and investigated the effects of various conditions on a SW such as motionless water depth and the paddle’s velocity. They realized that the faulty fitness of WP to the penstock has a great effect on SW height. Ren *et al.* (2019) investigated a SW interface with a sunken breakwater. In this study, they applied the reliable particle technique (CPM) to obtain the contours of a SW when it collided with a sunken breakwater. The CPM model projected the wave elevations, contours, and speeds with better accuracy. You *et al.* (2019) numerically perused SW interaction with a flat plate. They employed a limited interpolation shape to make a multiphase mathematical viscous wave flume for the nonlinear relation between SWs and a sunken plane plate and used a tangent of hyperbola aimed at the interface capturing structure for the free-surface elevation. The researchers considered various conditions such as submergence depths and SW heights. The hydrodynamic forces’ results were obtained under various conditions. Seiffert *et al.* (2014) numerically investigated the interactive relationship between a SW and a plane plate. They calculated horizontal and vertical forces employing Open FOAM in a 2D numerical wave tank (NWT). The researchers carried out simulations of SW relation with a plane plate at various water depths, submergence depths below and altitudes above the SWL, and wave amplitudes. Eren *et al.* (2020) numerically researched the collision between a SW and a dynamic chamber. The researchers applied a 2D NWT with a piston-type wave-producer to produce the SW. The renormalization group (RNG) turbulence model and the volume of fluid (VOF) model were evaluated in this study. The researchers obtained free-surface deformation and hydrodynamic forces values using

the Ansys Fluent commercial software. Breakwaters’ influence on SWs’ propagation was numerically studied by Tsai *et al.* (2016). The RNG turbulence model was integrated into the RANS equations in this study, which showed that breakwater height significantly affects SWs’ entrainment on the sloping terrain. Zhang *et al.* (2019) numerically investigated a rectangular floating breakwater’s heave motion. They discussed the floating breakwater’s hydrodynamic behavior and wave energy absorption, simulated using Ansys Fluent. This study showed that heaving performance and wave energy converters significantly depend on incident wave conditions and submergence depth. Qu *et al.* (2017) used a floating breakwater to decrease the hydrodynamic load on a bridge deck considering the effect of a conical wave. The researchers defined a 2D NWT to solve the incompressible two-phase flow by applying the open-source flow solutioner REEF3D. In their study, the effects of wave height, water depth, immersion depth, spacing distance, and the breakwater’s aspect proportion on reducing hydrodynamic behavior were considered. Zhan *et al.* (2017) computationally studied the relationship between inverse T-sort free-surface breakwaters and uniform and nonuniform waves. To solve the flow domain, the researchers applied RANS equations with the laminar method. The researchers presented the sway, heave, and pitch motions of an inverse T-type floating breakwater. To understand wave reflexion, wave transmission, and wave dissipation effects, the researchers compared the results for the floating breakwater and those for a fixed breakwater. Peng *et al.* (2013) numerically perused relations between water waves and inclined-moored immersed floating breakwaters. They used the direct-forcing submerged boundary technique and the VOF method to solve relations between water waves and circular and rectangular floating breakwaters. The researchers investigated the rectangular and round floating breakwaters’ surge, heave, and pitch motions and compared them with those observed in other experimental studies. Liu and Wang (2020a, 2020b) numerically investigated different characteristic sunken box-type floating breakwaters. They evaluated the smoothed particle hydrodynamics (SPH) technique to study simulated floating breakwaters’ motion. The researchers chose dual rectangular, single rectangular, dual round, and single round breakwaters for case studies using SPH. The numerical outputs revealed that breakwaters’ immersion depths affect their performances. A new version of the incompressible smoothed particle hydrodynamics (ISPH) model was improved by Liu *et al.* (2020). The model could solve fluid-structure interaction and moving body problems with high accuracy. The researchers used the mirror particle method for solving the moving boundary. Different numerical experiments were carried out for model validations such as water entry of cylinder, symmetric wedge, and rigid cube falling. The results showed that this model was very effective for simulations of these kinds of problems. Chen *et al.* (2020) studied vertical-pile-restrained wave energy converter sort floating breakwaters. They optimized the floating breakwaters’ profiles to absorb extra wave energy and less wave transmission. The

researchers employed RANS formulas employing the particle-in-cell technique combined with a Cartesian cut cell-based robust coupling procedure in this study. The results illustrated that a rectangular enclosure with a small curve in the corner could absorb more wave energy. Cheng and Lin (2018) used the virtual boundary force (VBF) technique to study the interaction between water waves and a moored floating body. They simulated the movements of a free-floating box in two dissimilar water waves for validation. They then investigated a catenary moored floating structure's wave-caused movements using the VBF method. Ji *et al.* (2017) numerically and experimentally investigated cylindrical double pontoon-in floating breakwaters. A 2D fully nonlinear NWT was applied for numerical simulations using the higher-order boundary component technique and mixed Eulerian-Lagrangian. The researchers obtained the hydrodynamic forces' outputs and compared them to those of other numerical methods and experimental studies. Nikpour *et al.* (2019) experimentally evaluated trapezoidal pontoon-type floating breakwaters in deep water. The researchers measured the floating breakwaters' motion and hydrodynamic forces on the uniform wave diminution under different sea state circumstances, such as varying incident wave heights and wave frequencies. They realized that a trapezoidal floating breakwater is more effective than a rectangular floating breakwater because it more effectively reduces the wave spread and mooring line force. Ning *et al.* (2017) applied an analytical method to calculate 2D couple-pontoon floating breakwaters' hydrodynamic forces. To find an effective frequency range, they investigated the relationship between geometric parameters and hydrodynamic forces. They compared the dual-pontoon breakwater and the single-pontoon one, and the results illustrated that the dual-pontoon breakwater's influential frequency range was wider than that of the single-pontoon breakwater when they have the same total volume. Hu *et al.* (2017) numerically investigated interactions between waves and a round cylinder during the submerging procedure. They used Ansys Fluent to solve RANS relations and apply the VOF method. The researchers monitored the free surface deformation and the pressure variances in the chamber throughout the immersion process. Using a 2D NWT, they calculated hydrodynamic forces on the round chamber through dissimilar wave effect angles, wave heights, and wave frequencies. Tian *et al.* (2018) numerically and experimentally studied a submerged cylinder under waves' effects. They calculated the submerged cylinder's hydrodynamic force from waves of dissimilar heights and frequencies in a 3D NWT. Ansys Fluent provided this study's results. The researchers employed a user-defined file (UDF) to generate a Stokes second-order wave in the velocity inlet boundary condition. Comparison between results indicates high consistency between numerical simulations and experimental studies. Olcay *et al.* (2016) numerically evaluated a real squid's hydrodynamic forces. They used the realizable k-ε turbulence model to calculate drag and lift forces under various locomotion conditions: dissimilar attack angles, Reynolds numbers, and

funnel diameters. The Ansys Fluent software produced the simulations' results.

The existing work is a continuation of the authors' former work (Eren *et al.* 2020). Here, we have used Ansys Fluent for modeling three different SWs and three different floating breakwaters. Floating breakwaters don't bind anywhere and they don't have initial speed, and they can move in two different directions when WS act on them. Floating breakwaters float on the free surface. In this work, three different wave heights were applied (0.1, 0.2, and 0.3 m), three different floating breakwaters shapes were applied (square breakwater, circular breakwater, and modified breakwater), and two different densities of floating breakwaters were studied. In the previous one, one wave height was applied (0.1m), a moving circular cylinder with two constant velocities was studied ($u=0.05$ m/s and 0.1m), and the circular cylinder does not have density.

In the current study, we evaluated three different floating breakwater interactions with three different SWs in the NWT to understand floating breakwaters' motions and kinetic energy and the horizontal and vertical forces on these breakwaters during varied SW acts. Two dissimilar UDF codes were evaluated for generating SWs and the floating breakwater's motions in the NWT. To control the codes' correctness and ability, the researchers initially confirmed the numerical codes to make SWs and floating breakwaters movements in the NWT considering other numerical simulations, analytic methods, and experimental studies. Additionally, three dissimilar models of floating breakwaters were described and unraveled in three SWs. Interaction of floating structures with waves is highly important, and this study can help us predict floating structures' motions considering different wave heights and analyze waves' forces to design floating structures and control and use wave energy. Moreover, tsunami waves behave like SWs; for this reason, this study helps us understand floating breakwaters' behaviors against tsunami-like SWs and design floating breakwaters that can absorb maximum wave energy. In addition, the accuracy and capability of this model were proved for the simulation interactions between waves and floating structures.

2. COMPUTATIONAL TECHNIQUE

2.1 Leading Equations

We applied a 2D study containing water and air domains which were divided by a free surface boundary. We used the RNG k-ε turbulence one to solve the turbulent flow as given in Eren *et al.* (2020), Tian *et al.* (2018) and ANSYS, Inc. (2013), because it can model complex shear flows and improve solutions' accuracy. The governing formulas including the continuity and momentum equations are written as follows:

$$\frac{\partial \rho}{\partial t} + \frac{\partial(\rho u_i)}{\partial x_i} = 0 \quad (1)$$

$$\frac{\partial(\rho u_i)}{\partial t} + \frac{\partial(\rho u_i u_j)}{\partial x_j} = -\frac{\partial P}{\partial x_i} + \rho g_i + \frac{\partial}{\partial x_j} \left[\mu \left(\frac{\partial u_i}{\partial x_j} + \frac{\partial u_j}{\partial x_i} \right) \right] + S_i \quad (2)$$

The Transport model belonging to the RNG $k-\epsilon$ turbulence is expressed as:

$$\frac{\partial}{\partial t}(\rho k) + \frac{\partial}{\partial x_i}(\rho k u_i) = \frac{\partial}{\partial x_j} \left[\alpha_k \mu_{eff} \frac{\partial k}{\partial x_j} \right] + G_k + G_b - \rho \epsilon - Y_M + S_k \quad (3)$$

$$\frac{\partial}{\partial t}(\rho \epsilon) + \frac{\partial}{\partial x_i}(\rho \epsilon u_i) = \frac{\partial}{\partial x_j} \left[\alpha_\epsilon \mu_{eff} \frac{\partial \epsilon}{\partial x_j} \right] + C_{1\epsilon} \frac{\epsilon}{k} (G_k + C_{3\epsilon} G_b) - C_{2\epsilon} \rho \frac{\epsilon^2}{k} - R_\epsilon + S_\epsilon \quad (4)$$

The RNG $k-\epsilon$ turbulence model's coefficients are $C_{1\epsilon}=1.42$, $C_{2\epsilon}=1.68$, and $C_{\mu}=0.09$.

10^{-6} was chosen for the criteria value of convergence of governing equations. We employed the VOF technique to calculate free surface deformation [Shen *et al.* \(2004\)](#). The computational cell is determined by the volume fraction of the phase α . Regarding the computational fluid, if $\alpha=1$, the cell has water. If $0<\alpha<1$, the cell considers the boundary between air and water.

$$\sum_{q=1}^n \alpha_q = 1 \quad (5)$$

The volume fraction's 2D continuity formula is shown below:

$$\frac{\partial \alpha_q}{\partial t} + u \frac{\partial \alpha_q}{\partial x} + v \frac{\partial \alpha_q}{\partial y} = 0 \quad (6)$$

2.2 Numerical Wave Tank (NWT)

The 2D NWT is illustrated in Figure 1a. The NWT was 80 m long and 2 m deep. A piston-type wave-maker was placed on the NWT's right side for the production of a SW, and a floating breakwater was positioned approximately 40 m from the paddle. The floating breakwaters had three shapes, so three floating breakwater models were defined: the square breakwater (Model 1), the circular breakwater (Model 2), and the modified breakwater (Model 3). Three different floating breakwaters were studied at two different densities of 800 and 900 kg/m³. The SW heights (H) are 0.1, 0.2, and 0.3 m with a fixed water depth (h) of 1 m in the NWT. This paper investigates a total of 18 cases (three different floating breakwaters with two different densities encountering SWs of three dissimilar heights). In the NWT, the floating breakwater wall and the tank bed floor had no-slip conditions. The top boundary is

described as having a "pressure inlet" condition; thus, air can pass into or out of the solution domain. The correct boundary is described as a "pressure outlet". In the current numerical study, we developed two UDF codes. One of them was employed for a piston-type wave-maker that creates a SW and the other was evaluated for the floating breakwater's movement. The floating breakwater can move in the x and y directions after being touched by the SW. Details of the floating breakwater models' cross-sectional shapes are illustrated from Fig. 1b to Fig. 1d. The numerical simulations' headnote is shown in Table 1.

It should be noted that wave heights from 0.1 to 0.3 m with a flow depth of 1 m are considered in this work, thus the ratio is 0.3 m as a maximum one. These are called linear SWs, however, the behavior of nonlinear SWs, when they interact with the floating breakwaters, will be different from each other. To work with the nonlinear options, the wave heights of 0.5-0.7 should be tested. Detailed information can be obtained from [Liang *et al.* \(2017\)](#).

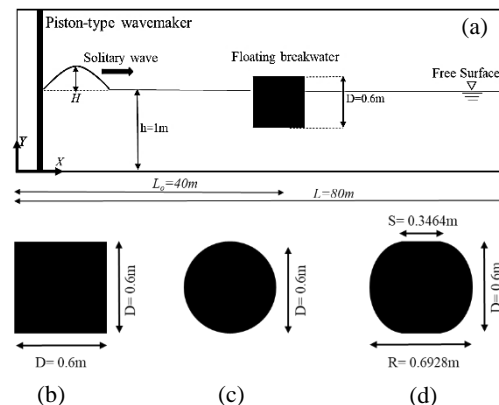


Fig. 1. Representation of the analyzed wave tank numerically (NWT) (a), features of the models coded as Model 1 (b), Model 2 (c), and Model 3 (d).

2.3 Spatial and Temporal Discretization

In the solution domain, we used triangular and quadrilateral elements. The solution domain was subdivided into various parts according to the multi-block mesh configuration method. Triangle mesh with high density was employed around the floating breakwater for simulation of the floating breakwater's locomotion using the dynamic mesh

Table 1 Computational simulations evaluated in the current study.

Model	Floating breakwater shape	Floating breakwater density (kg/m ³)	Floating breakwater mass (kg)	Wave Height H (m)	Water Depth h (m)
Model 1	Square	800, 900	288, 324	0.1, 0.2, 0.3	1
Model 2	Circular	800, 900	226.08, 254.34	0.1, 0.2, 0.3	1
Model 3	Modified	800, 900	284.2, 319.725	0.1, 0.2, 0.3	1

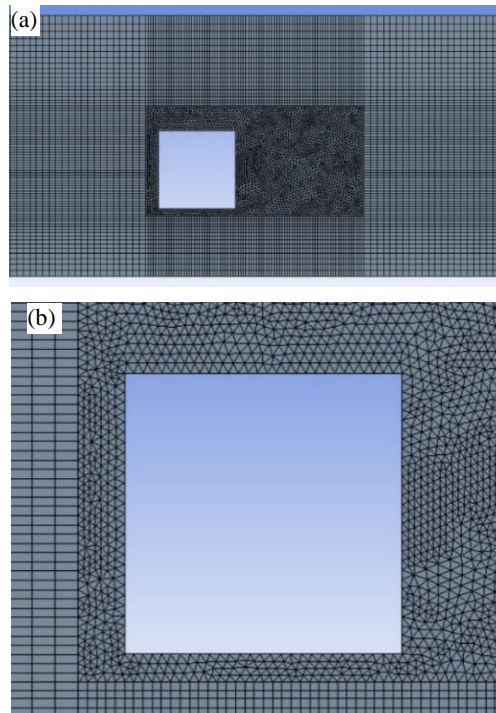


Fig. 2. Mesh of the solution domain (a), and its magnified detail around the cylinder surface (b).

method. The quadrilateral mesh was utilized for other parts of the solution domain. As illustrated in Fig. 2, a total of 125,000-190,000 elements were applied for three different models in the solution domain. A mesh convergence work was carried out for the computational domain Table 2 represents the alteration of maximum positive force with the dissimilar numeral of elements. In a conclusion, almost 125,000 elements were required for the models with a wave height of 0.1 m, and nearly 190,000 elements were required for models with a wave height of 0.3 m to keep the error of mesh less than 1%.

We have used the Courant–Friedrichs–Lewy condition to calculate the minimum time step so high numerical convergence could be obtained. We calculated Δt as follows:

$$\frac{u\Delta t}{\Delta x} \leq C \quad (7)$$

We used 0.25 as the VOF model’s Courant number. In this study, we selected $\Delta t = 0.001$ s to achieve high numerical reliability. Mesh convergence and the minimum time step studies help us to calculate forces

and capture free surface deformations with high accuracies. All numerical simulations were conducted on a Core i7-7700-based workstation that was working on Win10. Table 3 presents all cases’ calculation times for 26,000-time steps ($t = 26$ s).

Table 2 Mesh convergence work for the numerical domain

Mesh resolution (Model 3)	Maximum positive forces	% difference
100000	312	19.23
140000	252	13.49
160000	218	5.27
185000	206.5	0.72
190000	205	0

2.4 Eventuation of Solitary Wave and its Confirmation

WP movement can produce a SW at a constant water depth. According to Lin (2006, 2007) and Eern *et al.* (2020), we used a SW generation performance and fulfilled validation in this study. The paddle motion and free surface displacement, respectively, can be represented as:

$$u[x(t), t] = \frac{c\eta}{h+\eta} \quad (8)$$

$$\eta[x(t), t] = H \operatorname{sech}^2 \left\{ \sqrt{\frac{3H}{4h^3}} [x(t) - ct + x_0] \right\} \quad (9)$$

where x_0 is the space between the origin and wave crest at $t=0$, $x(t)$ is the location of the paddle at time t ($x(t) = \int_0^t u dt$), and c is the wave’s phase speed ($c = \sqrt{g(h+H)}$). We evaluated a UDF for paddle motion following the above formulas with the dynamic mesh technique for mesh transformation. The SW was generated with $H = 0.1$ m at fixed $w = 1$ m. The calculation area was 100 m long and 2 m deep. We employed a uniform mesh with $\Delta x = 0.1$ m and $\Delta y = 0.01$ m. We chose a fixed $\Delta t = 0.02$ s for time steps. The evaluation of the free-surface elevation’s time history is presented in Figs. 3a and 3b.

2.5 Free Decay of a Heaving Round Cylinder

To confirm the performance of the current numerical model for floating bodies’ heaving movement, we investigated a solid round cylinder floating on the free surface. We developed a UDF code for solving

Table 3 Calculation time and details of the mesh according to studied models

Models	0.1 m	Wave height 0.2 m	0.3 m
Model 1	22 h (90000 mesh elements)	27 h (105000 mesh elements)	34 h (122500 mesh elements)
Model 2	22 h (90000 mesh elements)	27 h (105000 mesh elements)	34 h (122500 mesh elements)
Model 3	22 h (90000 mesh elements)	27 h (105000 mesh elements)	34 h (122500 mesh elements)

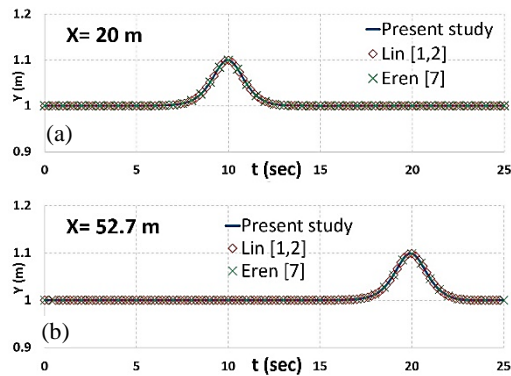


Fig. 3. An evaluation of the time past of the free-surface elevation at $x = 20$ m (a), $x = 52.7$ m (b).

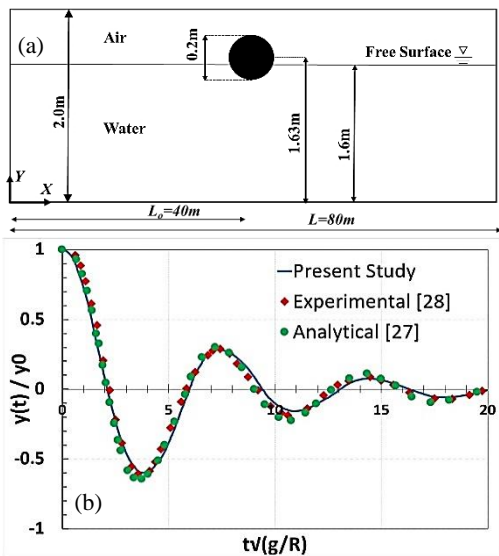


Fig. 4. dimensions of the computational domain (a), the cylinder center position as a relation to the non-dimensional time (b).

floating bodies' motion in the NWT. The round cylinder's heaving movement was computed in the NWT, and the outputs align with other analytical and experimental results by Maskell *et al.* (1970) and Ito (1977). Fig. 4a shows the computational domain for a heaving circular chamber's free decay in the motionless water tank. The solid circular cylinder's radius (R) is 0.1 m in a water depth (d) of 1.6 m ($d/R = 16$). The solid cylinder's density is 500 kg/m^3 . The solid cylinder's gravity center was approximately 0.03 m from the free water's surface. The solid cylinder was placed at a long NWT to prevent any free surface wave reflection during the investigation. The solid cylinder started to slosh in a heaving motion till the cylinder and water returned to the equilibrium state in a quiescent state. It can be observed that the cylinder had a harmonic oscillatory movement in time with fading amplitude. Fig. 4b presents the comparison between the motion of the cylinder's midpoint concerning the non-dimensional time and other analytical and experimental results. The present numerical simulation results agree well with other results. Fig. 5 represents free surface deformation when the cylinder was in oscillatory

movement. The numerical results show that the codes have high accuracy a(a)capability for a SW's occurrence and floating bodies' motion.

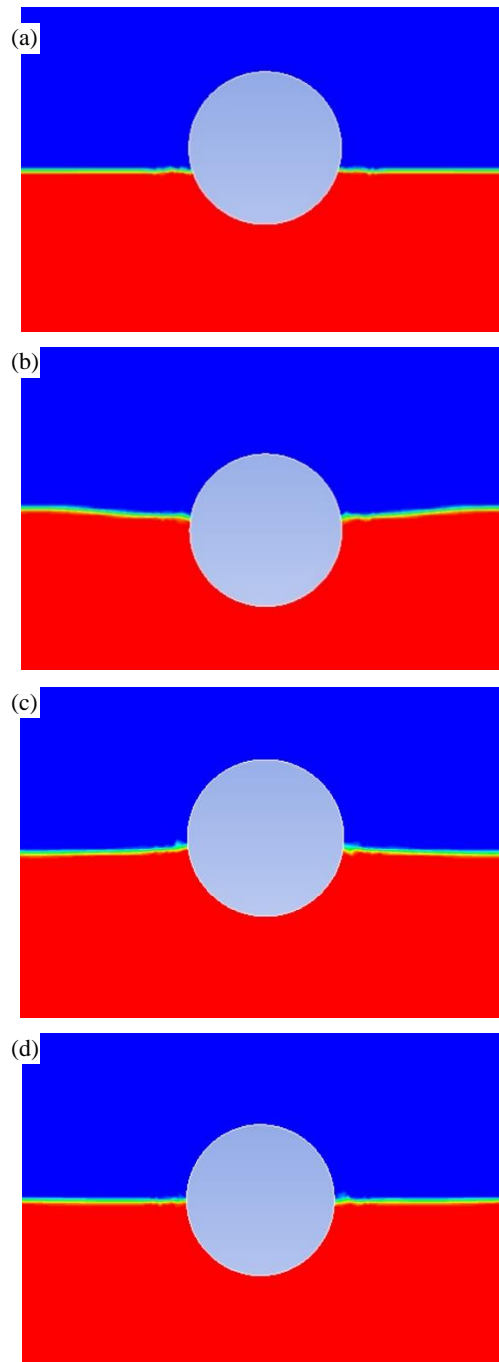


Fig. 5. Views of the circular cylinder oscillatory motion as a function of the non-dimensional time on the free surface of a still water (a) $t\sqrt{g/R} = 0.0$, (b) $t\sqrt{g/R} = 4.0$, (c) $t\sqrt{g/R} = 7.35$, (d) $t\sqrt{g/R} = 20.0$

It should be noted that there are two comparison studies with analytical solutions and experimental measurements on wave creation (Fig. 3) and free motion of a heaving round cylinder (Figs. 4 and 5). Firstly, we validated our model with two

workbenches as the generation of a SW evaluating the WP movement and free motion of a heaving round chamber on the free surface of motionless water. These sections (2.4 and 2.5) show the ability of this model for solving wave structure interaction problems. Then, we used it for modeling the interaction of three different waves with three different floating structures. Validation of one geometry of cylinder was performed as the most common configuration in numerical works in the literature. Validating another shape can be considered for emphasizing the reliability of the work as existed in [Yu *et al.* \(2021\)](#) and [Zheng *et al.* \(2018\)](#).

3. RESULTS AND DISCUSSION

3.1 Motion Responses

During excitation by a SW, floating breakwaters can freely move in two degrees of freedom—namely, heave motion in the y-direction and sway motion in the x-direction. The time orders of the displacements of floating breakwaters' mass centers, which are heave and sway motions, respectively, are represented in Figs. 6 and 7. We compared floating breakwater Models 1, 2, and 3 under the conditions of three different SW heights and at two densities (800 and 900 kg/m³). Because we used two densities for the current work's models, the mass center of the floating breakwaters with 900 kg/m³ density was initially placed lower than that of those with 800 kg/m³ density at the still water level. It should be noted that we placed the floating breakwater at a distance of approximately 40 m from the paddle, so the breakwater's sway motion starts here. When the SW acted on the floating breakwater, the breakwater started to move upward and to the right until the SW's peak arrived at the floating breakwater, meaning that the breakwater's heave and sway movements gradually increased. When the SW reached the floating breakwater, the main wave crest separated into two parts, at which point the floating breakwater reached its maximum height. The floating breakwater began to travel down immediately after the SW's peak passed it, meaning that the floating breakwater's heave and sway movements gradually diminished. Finally, the floating breakwater achieved static equilibrium after the SW completely passed it. Finally, square floating breakwaters can return to their equilibrium state at rest earlier than other models because of their square corners.

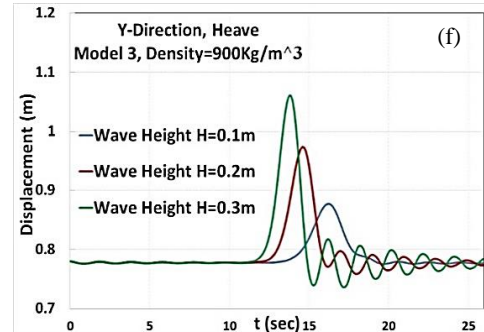
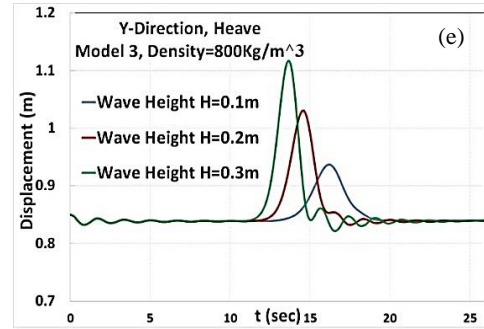
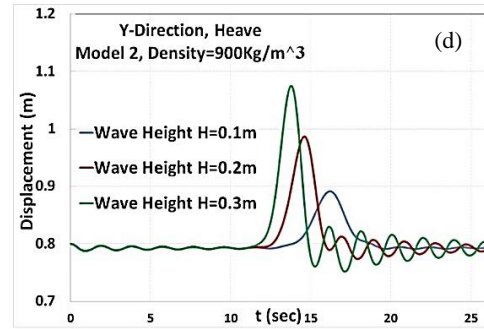
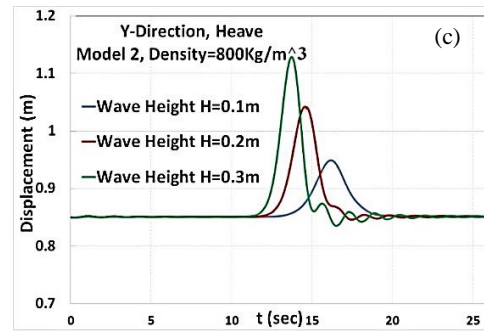
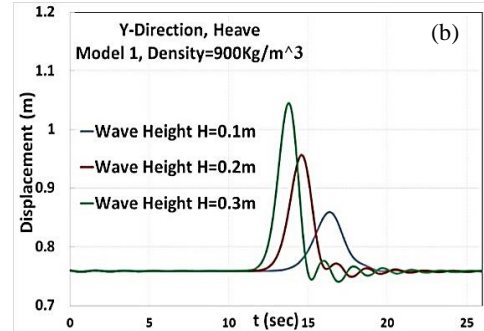
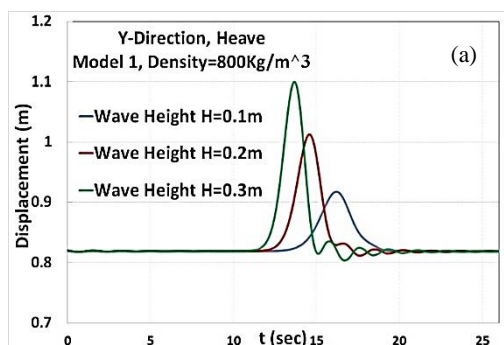


Fig. 6. Time alteration of the heave motion displacement under three various SW heights for models 1 (a,b), 2 (c,d), and 3 (e,f) considering densities of 800 and 900 kg/m³.

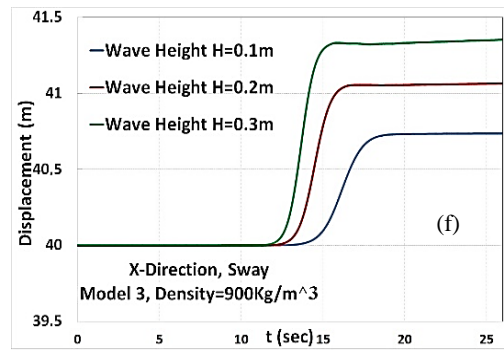
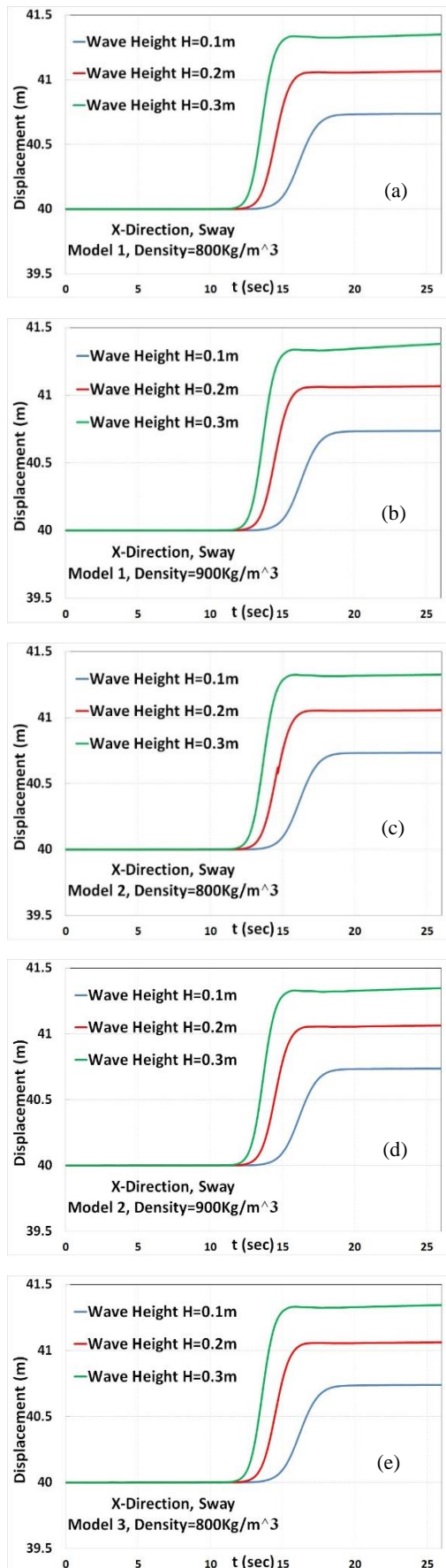


Fig. 7. Time variation of the sway motion displacement under three various SW heights for Models 1 (a,b), 2 (c,d), and 3 (e,f) considering densities of 800 and 900 kg/m³.

Wave height has a direct effect on floating breakwaters' heave and sway motions. It should be noted that heave and sway motions increase and further displacements can be achieved with increased wave height. In addition, the height of the heave motion and that of the SW are nearly the same. SWs with the same wave height have the same effects on all models' heave motions.

The floating breakwaters' heave motions when coming into contact with the SW with a height of 0.3 m were about 66.6% larger than those of the breakwaters contacting the wave with a height of 0.1 m. The SW with a wave height of 0.3 m can move faster than SWs of 0.1 and 0.2 m heights. This is because the vortices around the floating breakwater, as well as the strength of their shedding, under the wave with 0.1 m height. The forward sway distance with a wave of 0.3 m height was greater than the forward sway distance with a wave of 0.1 m height. The sway motion of the floating breakwaters under the SW of 0.3 m height was about 50% bigger than that of the breakwaters under the wave with a height of 0.1 m. In general, the breakwaters' sway motions were larger than their heave motions.

3.2 Hydrodynamic Forces

Hydrodynamic forces can appear on a floating structure once it travels in a fluid medium (Olcay *et al.* 2016, Batchelor 2000, Vasudev *et al.* 2014 Tabatabaei-Malazi *et al.* 2020) and are determined via the following formulas:

$$F_{Horizontal\ Force} = F_{D_pressure} + F_{D_viscous} = \oint P \hat{n} \cdot \hat{e}_d dS + \oint \tau_w \hat{t} \cdot \hat{e}_d dS \quad (10)$$

$$F_{Vertical\ Forces} = F_{L_pressure} + F_{L_viscous} = \oint P \hat{n} \cdot \hat{e}_i dS + \oint \tau_w \hat{t} \cdot \hat{e}_i dS \quad (11)$$

where $F_{D_pressure}$ and $F_{D_viscous}$ are drag forces in the x-way owing to the pressure and viscous influences, respectively. In the same way, $F_{L_pressure}$ and $F_{L_viscous}$ are lift forces in the y-way caused by the pressure and viscous influences, correspondingly. At this point, τ_w is the wall shear stress on a floating breakwater's surface.

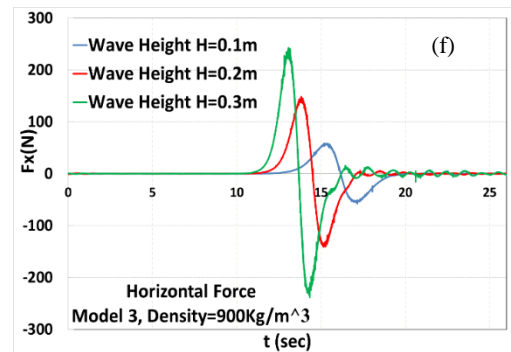
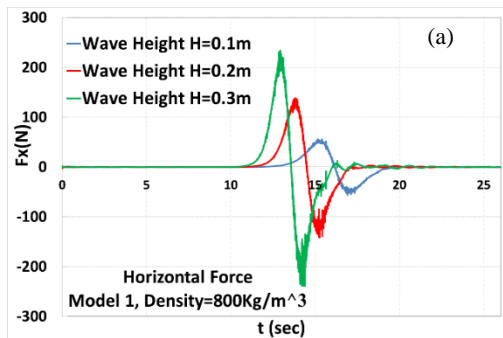
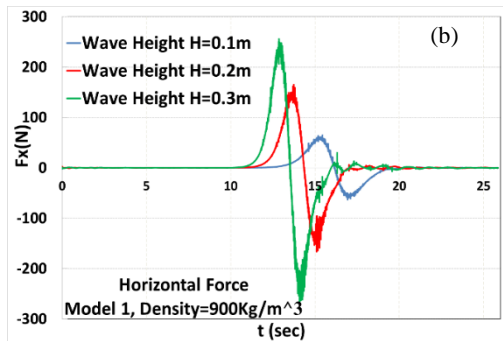
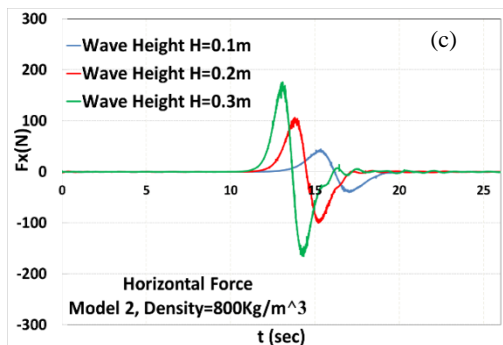


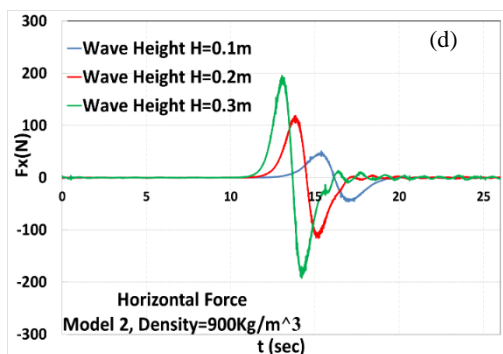
Fig. 8. Time alteration of the horizontal forces under various three SW heights for Models 1 (a,b), 2 (c,d), and 3 (e,f) densities of 800 and 900 kg/m³.



We computed the impact of the SWs' horizontal and vertical hydrodynamic forces on the floating breakwaters. The forces on the floating breakwater are calculated from a surface aggregation of the viscous and pressure influences such as hydrodynamic and hydrostatic pressures and shear stresses.



In Fig. 8, evaluations are represented for the time past of horizontal forces for three different models (Models 1–3) at two densities (800 and 900 kg/m³) and three-wave heights of 0.1, 0.2, and 0.3 m. Horizontal forces demonstrated similar behavior in all simulations. First, the horizontal force on the floating breakwater from the SW was near zero. The horizontal force changed when the SW reached and passed the floating breakwater. The horizontal force increased when the SW reached the floating breakwater. The horizontal force gradually decreased when the SW passed the floating breakwater.



For all models, two peaks were generated in the horizontal forces throughout the SW's action on the floating breakwater. The horizontal forces had positive and negative peaks in opposite directions. At this point, the maximum positive horizontal force is called the positive force (PF), and the minimum negative one is called the negative force (NF). The horizontal force peaks demonstrated similar behavior in all simulations. The floating breakwater absorbed the SW's energy once the wave passed the breakwater. The decrease or increase in horizontal forces depended on the floating breakwater's shape and density and the SW's height. The proportion of the floating breakwater's volume submerged within the water was greater for the breakwater with 900 kg/m³ density than for the breakwater with 800 kg/m³ density; thus, a considerable part of the denser floating breakwater could be contacted by the SW. It is understood that the horizontal force on the floating breakwater with 900 kg/m³ density always was greater than that on the floating breakwater with 800 kg/m³ density. Maximum horizontal forces occurred in Model 1 (Fig. 8a, 8b) for both densities because of the floating breakwater's shape. The square corners have the predominant factor to increase horizontal forces in Model 1. It can also be observed that the minimum horizontal forces occurred in Model 2

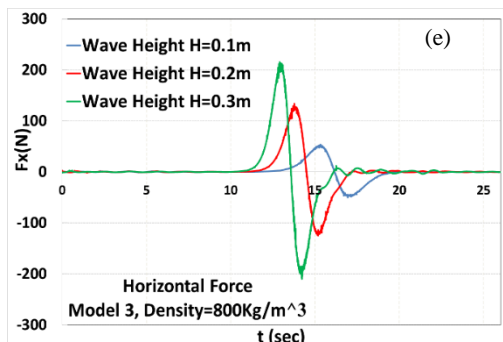


(Fig. 8c,8d) because of the floating breakwater's shape. The difference between the PF and NF in Model 1 was greater than those in Models 2 and 3. The negative horizontal force can appear in entire figures as a result of the pressure gradient. In other words, the pressure gradient is created in front of the cylinder once the SW passes the floating breakwater. The pressure gradient slowly vanishes afterward the SW passes the floating breakwater. Water reflux occurs behind the floating breakwater because the water travels to the negative pressure zone. Water reflux causes the flow to move in a negative direction. The negative flow acts on the floating breakwater to create the negative horizontal force.

It can be observed that Model 1's NF was larger than those of Models 2 and 3 because of the floating breakwater's square shape. Furthermore, the positive and negative horizontal forces of the floating breakwaters with 900 kg/m³ density are greater than the floating breakwaters with 800 kg/m³ density. It is also understood that the horizontal force of the SW with a height of 0.3 m was greater than that of the shorter SWs for all models. According to the obtained results, the impact of the horizontal force of the SW with a wave height of 0.3 m on the floating breakwater appeared earlier than those of the shorter SW for all models.

The horizontal forces' positive peaks are presented in Fig. 9. The maximum positive forces of Model 3 were greater than those of the other models. It also should be noted that the maximum positive forces of all models were nearly the same for waves of 0.1 m height, but these forces had great variation among the models at waves with heights of 0.2 m and 0.3 m. Tables 4 and 5 present the happening times of the maximum horizontal force when the solitary waves pass the structures.

Fig. 10 presents the time pasts of hydrodynamic forces acting on the floating breakwater vertically. The visual outcomes show the vertical forces without hydrostatic ones on the floating breakwater in the y-direction. Similarly, the figures illustrate hydrodynamic forces acting on the floating breakwater from the SW. The vertical forces had the same behavior in all models. The floating breakwater was at rest before the SW acted on it, so the vertical one from the SW was near zero. The vertical one started to rise after the SW contacted the breakwater. Model 1's vertical forces were larger than those of

the other models. The arrangements and figures of the vertical force's peaks were the same for all models. In all models, the vertical forces had many peaks, but the first three peaks for each model had the greatest magnitudes. The peaks disappeared when the floating breakwater and the water returned to their equilibrium state in a stagnant situation. In other words, the vertical force decreased to zero after the SW passed the floating breakwater.

3.3 Kinetic Energy

In Fig. 11, evaluations are presented for the time pasts of kinetic energy for Models 1–3 at two densities (800 and 900 kg/m³) and three-wave heights (0.1, 0.2, and 0.3 m). In all numerical cases, the breakwater's kinetic energy gradually increased when the SW arrived at the breakwater and gradually decreased after the SW passed it. It is observed that

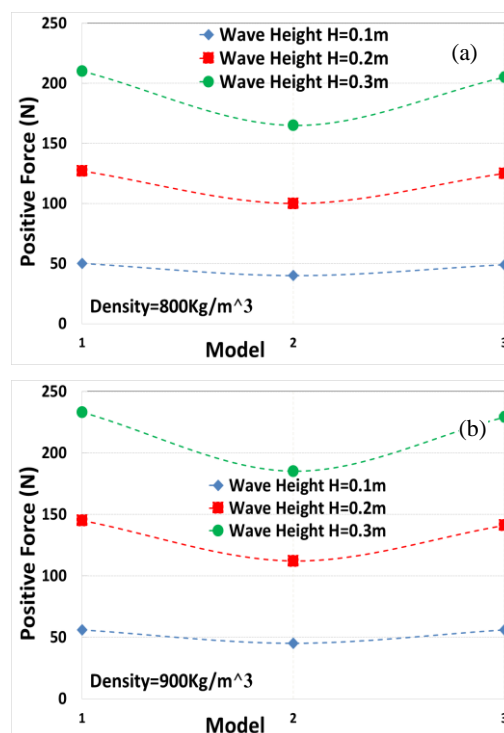


Fig. 9. Positive peaks of the horizontal forces for entire models considering densities of 800 (a) and 900 kg/m³ (b).

Table 4. The time of occurrence of the peaks of horizontal forces for density of 800 kg/m³.

Models	0.1 m	Wave height 0.2 m	0.3 m
Model 1	t=15.21 s	t=13.73 s	t=13.01 s
Model 2	t=15.33 s	t=13.86 s	t=13.08 s
Model 3	t=15.22 s	t=13.77 s	t=13.02 s

Table 5. The time of occurrence of the peaks of horizontal forces for density of 900 kg/m³.

Models	0.1 m	Wave height 0.2 m	0.3 m
Model 1	t=15.11 s	t=13.68 s	t=12.90 s
Model 2	t=15.29 s	t=13.76 s	t=13.02 s
Model 3	t=15.25 s	t=13.72 s	t=12.96 s

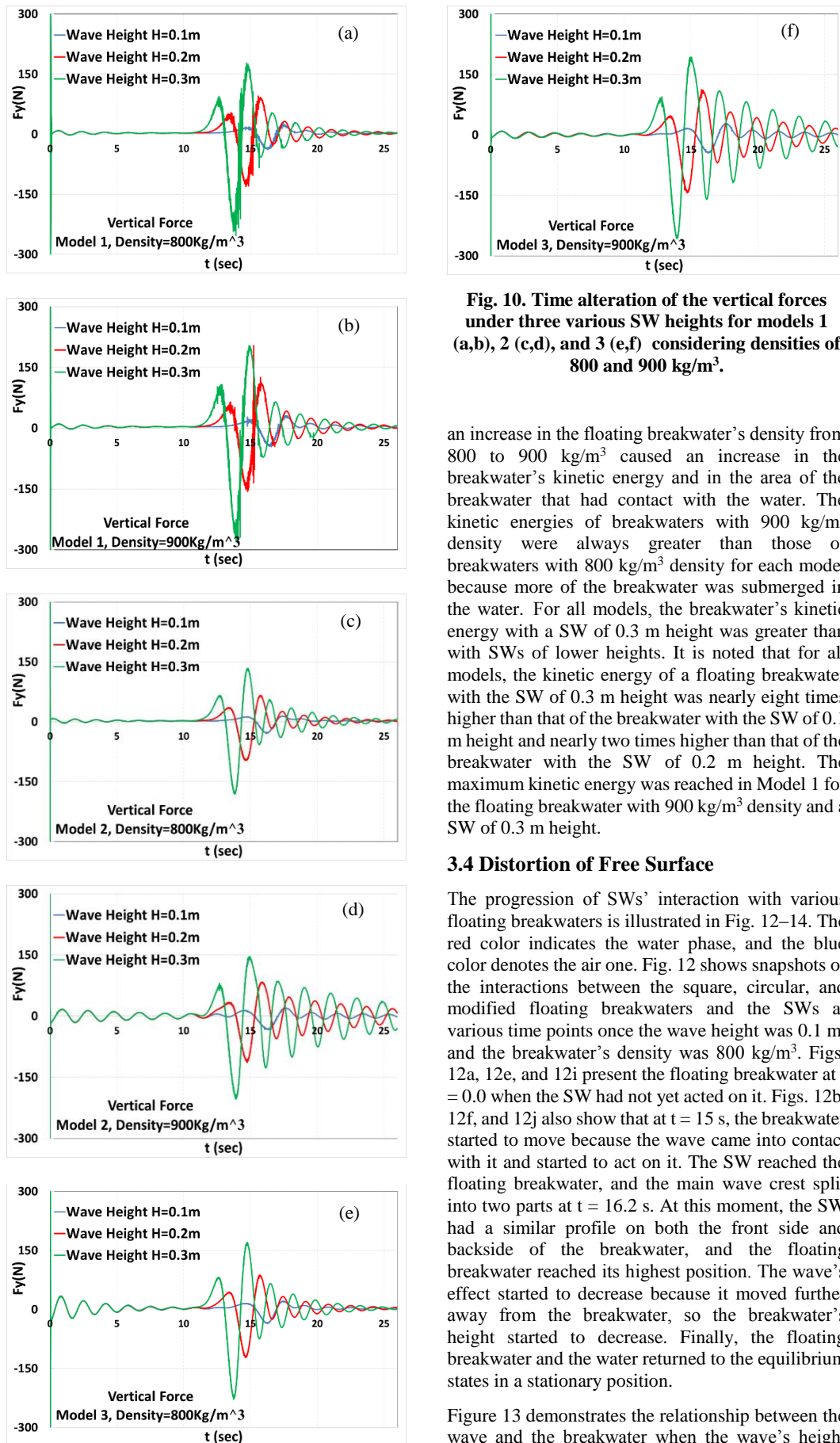


Fig. 10. Time alteration of the vertical forces under three various SW heights for models 1 (a,b), 2 (c,d), and 3 (e,f) considering densities of 800 and 900 kg/m³.

an increase in the floating breakwater's density from 800 to 900 kg/m³ caused an increase in the breakwater's kinetic energy and in the area of the breakwater that had contact with the water. The kinetic energies of breakwaters with 900 kg/m³ density were always greater than those of breakwaters with 800 kg/m³ density for each model because more of the breakwater was submerged in the water. For all models, the breakwater's kinetic energy with a SW of 0.3 m height was greater than with SWs of lower heights. It is noted that for all models, the kinetic energy of a floating breakwater with the SW of 0.3 m height was nearly eight times higher than that of the breakwater with the SW of 0.1 m height and nearly two times higher than that of the breakwater with the SW of 0.2 m height. The maximum kinetic energy was reached in Model 1 for the floating breakwater with 900 kg/m³ density and a SW of 0.3 m height.

3.4 Distortion of Free Surface

The progression of SWs' interaction with various floating breakwaters is illustrated in Fig. 12–14. The red color indicates the water phase, and the blue color denotes the air one. Fig. 12 shows snapshots of the interactions between the square, circular, and modified floating breakwaters and the SWs at various time points once the wave height was 0.1 m, and the breakwater's density was 800 kg/m³. Figs. 12a, 12e, and 12i present the floating breakwater at t = 0.0 when the SW had not yet acted on it. Figs. 12b, 12f, and 12j also show that at t = 15 s, the breakwater started to move because the wave came into contact with it and started to act on it. The SW reached the floating breakwater, and the main wave crest split into two parts at t = 16.2 s. At this moment, the SW had a similar profile on both the front side and backside of the breakwater, and the floating breakwater reached its highest position. The wave's effect started to decrease because it moved further away from the breakwater, so the breakwater's height started to decrease. Finally, the floating breakwater and the water returned to the equilibrium states in a stationary position.

Figure 13 demonstrates the relationship between the wave and the breakwater when the wave's height

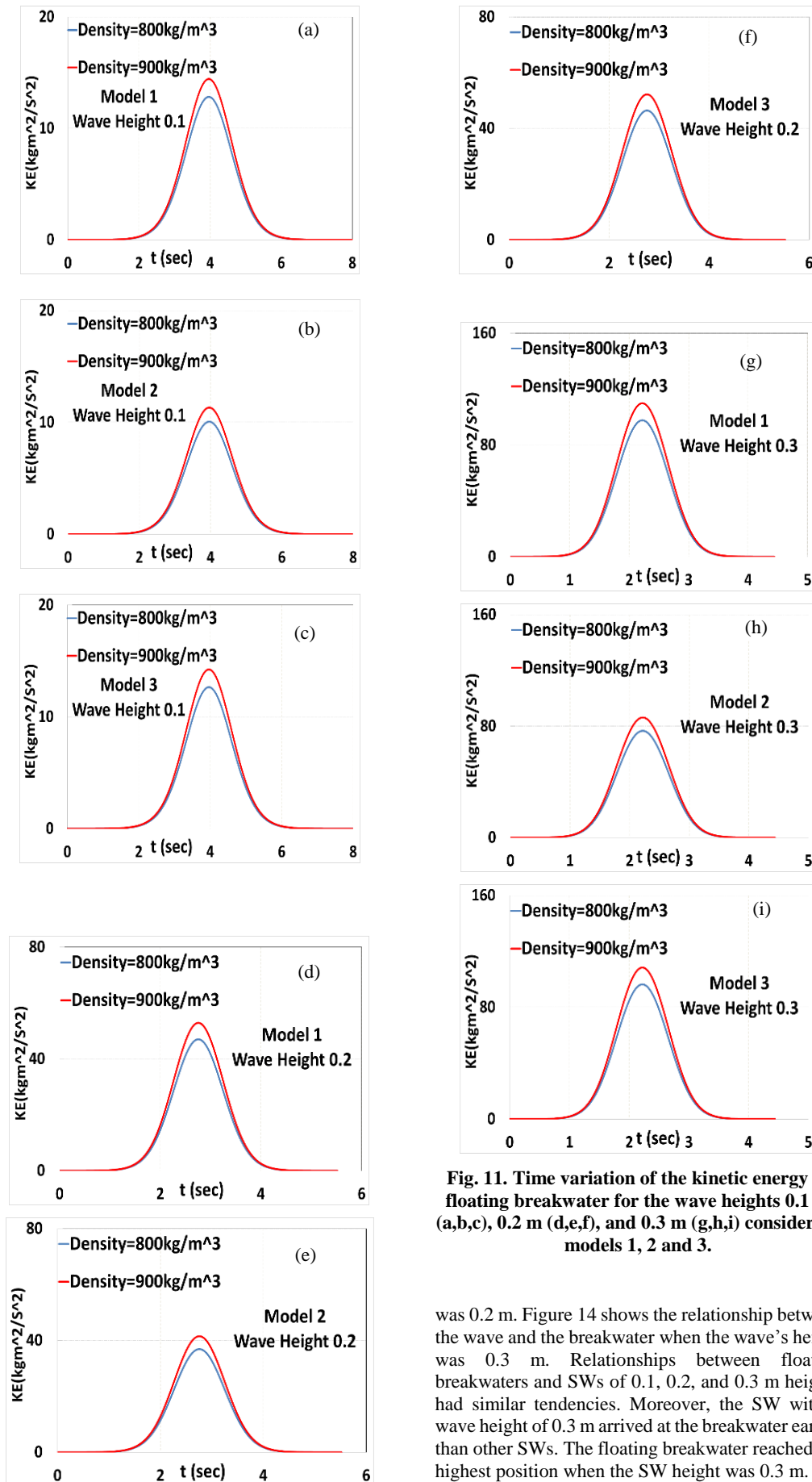


Fig. 11. Time variation of the kinetic energy of floating breakwater for the wave heights 0.1 m (a,b,c), 0.2 m (d,e,f), and 0.3 m (g,h,i) considering models 1, 2 and 3.

was 0.2 m. Figure 14 shows the relationship between the wave and the breakwater when the wave's height was 0.3 m. Relationships between floating breakwaters and SWs of 0.1, 0.2, and 0.3 m heights had similar tendencies. Moreover, the SW with a wave height of 0.3 m arrived at the breakwater reached earlier than other SWs. The floating breakwater reached the highest position when the SW height was 0.3 m.

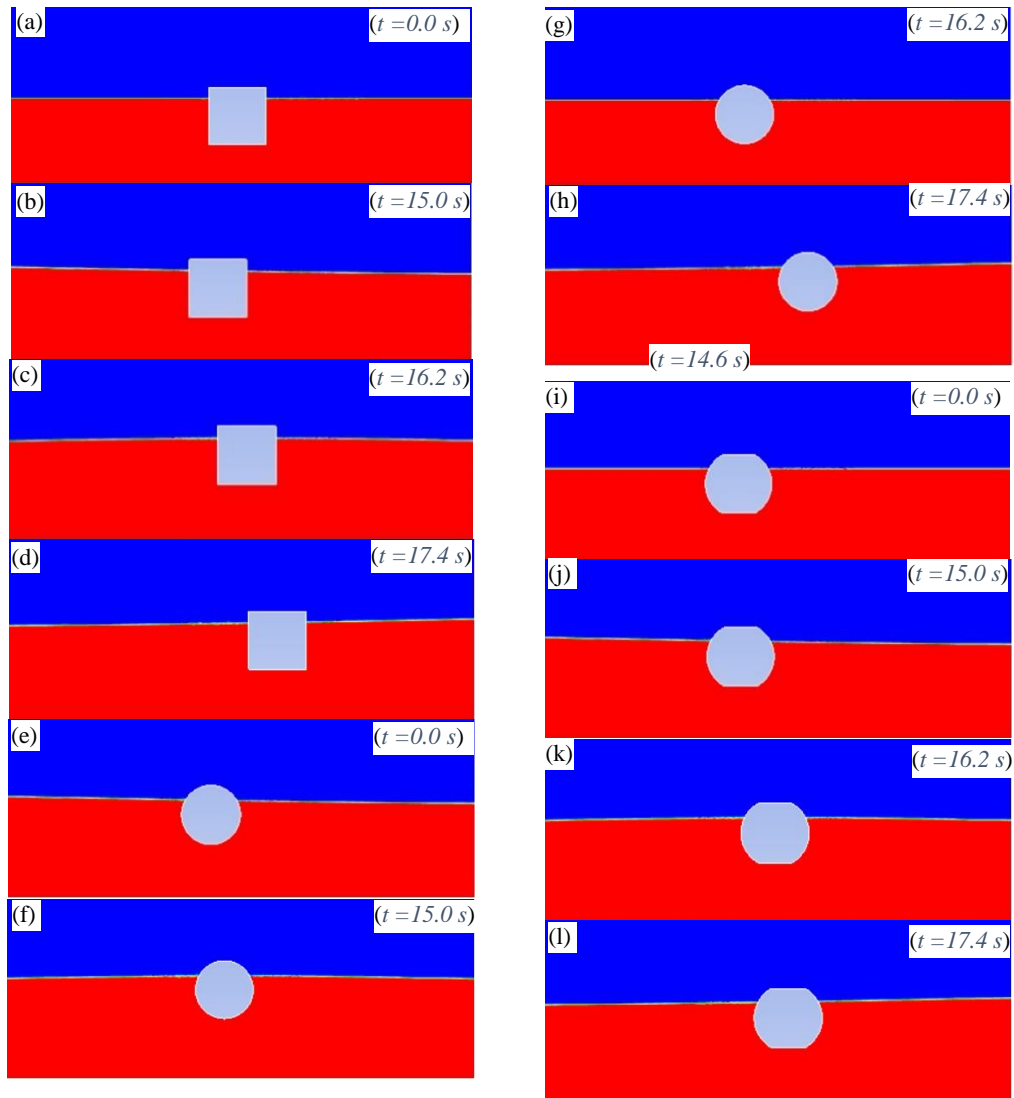
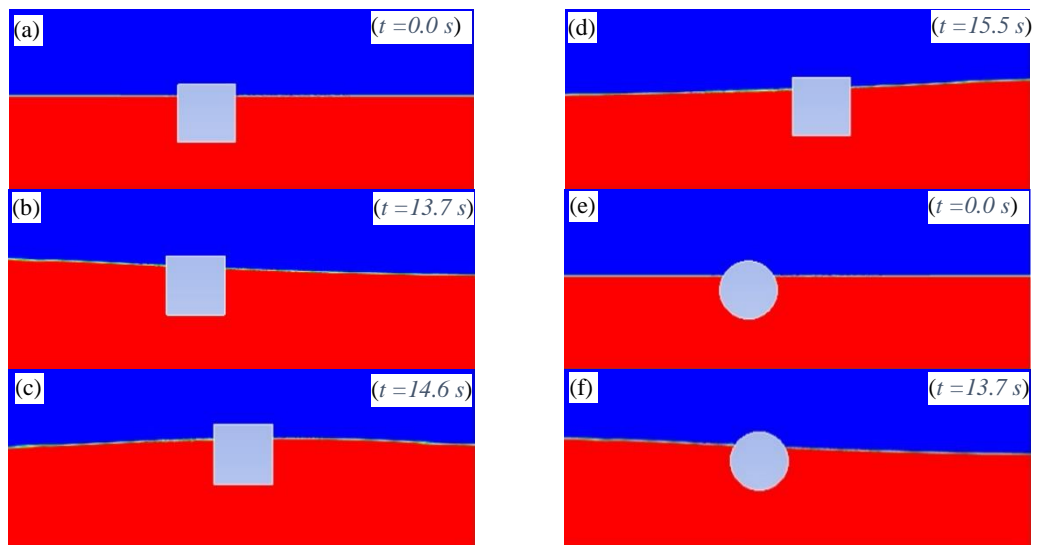


Fig. 12. View of development process of a SW relating with the floating breakwater for models 1 (a,b,c,d), 2 (e,f,g,h), and 3 (i,j,k,l) considering the SW height of 0.1 m related with $t = 0.0$ s, $t = 15$ s, $t = 16.2$ s and $t = 17.4$.



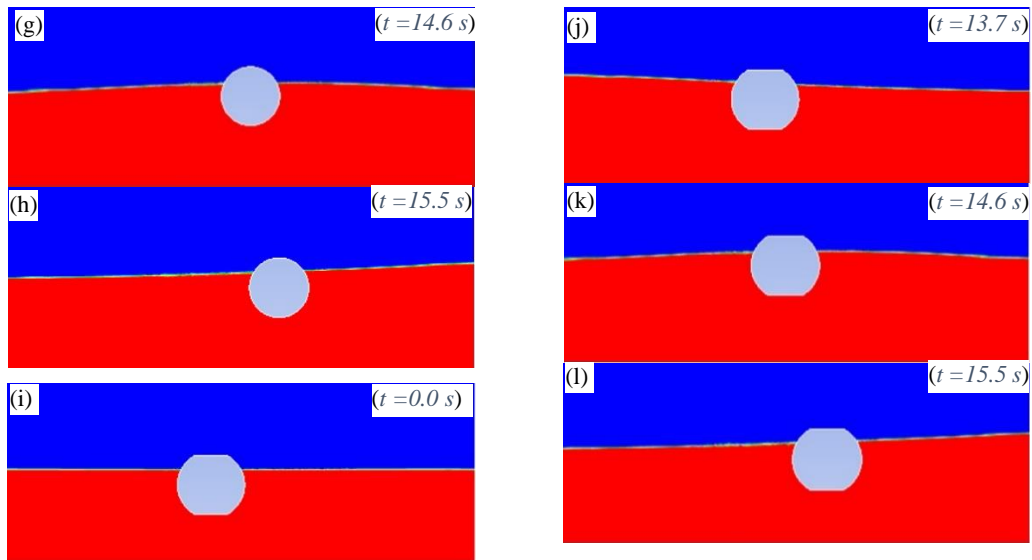


Fig. 13. View of development of a SW interacting with the floating breakwater for models 1 (a,b,c,d), 2 (e,f,g,h), and 3 (i,j,k,l) SW height of 0.2 m related with $t = 0.0$ s, $t = 13.7$ s, $t = 14.6$ s and $t = 15.5$ s.

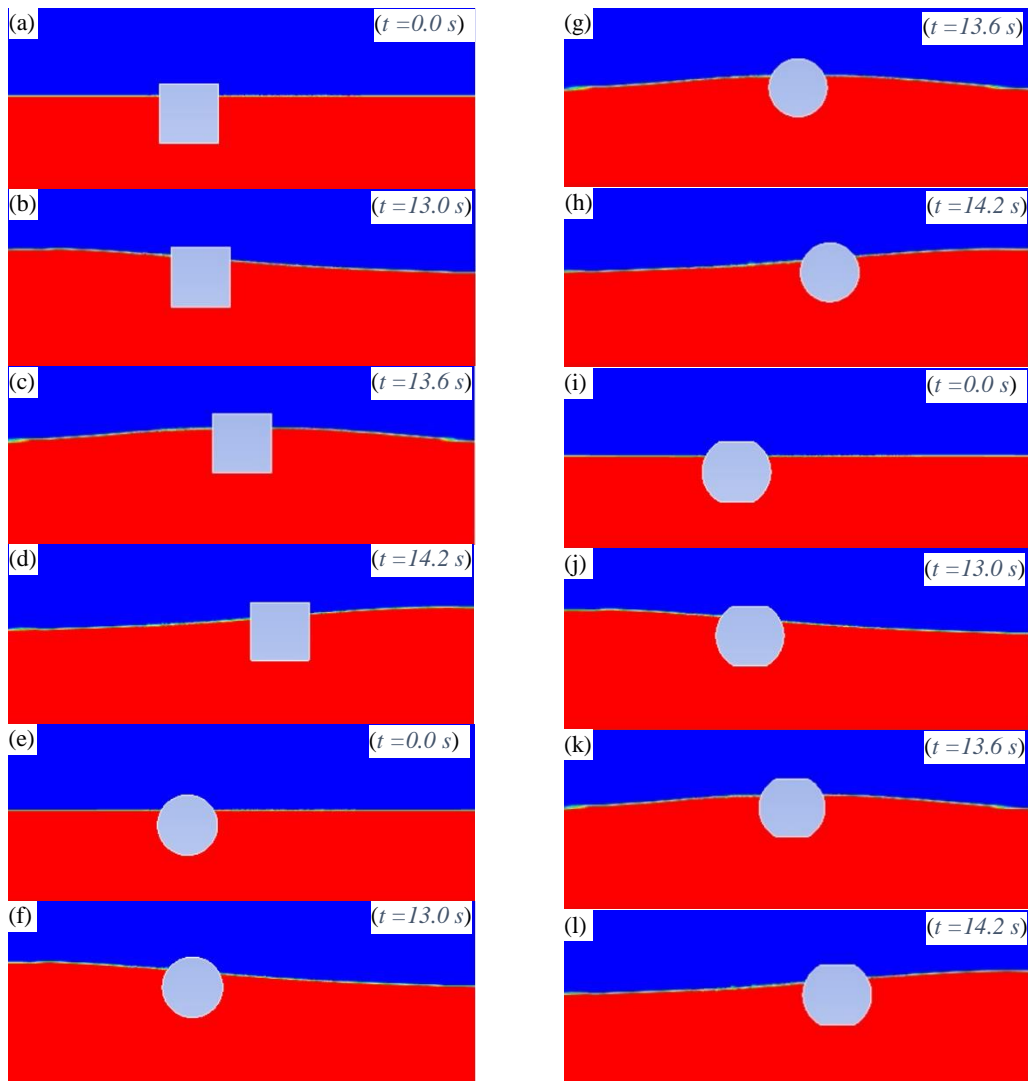


Fig. 14. View of development process of a SW relating with the floating breakwater for models models 1 (a,b,c,d), 2 (e,f,g,h), and 3 (i,j,k,l) considering the SW height of 0.3 m related with $t = 0.0$ s, $t = 13$ s, $t = 13.6$ s and $t = 14.2$ s.

3.5 Velocity Contours Plots of Numerical Study

The velocity contours around three different floating breakwaters that were plotted in Fig. 15-17. The Moments that SWs reached the floating breakwater when the floating breakwater reached its highest position were chosen for showing velocity contours. Fig. 15a, 15b, and 15c show velocity contours around the square, circular, and modified floating breakwaters at $t=16.2s$ at what time the wave height was 0.1 m and the breakwater's density was 800 kg/m^3 . Fig. 16a, 16b, and 16c present velocity contours around the floating breakwaters at $t=14.6s$ at what time the wave height was 0.2 m. velocity contours around the floating breakwaters at $t=13.6s$ are illustrated in Fig. 17a, 17b, and 17c at what time the wave height was 0.3 m. It was realized that

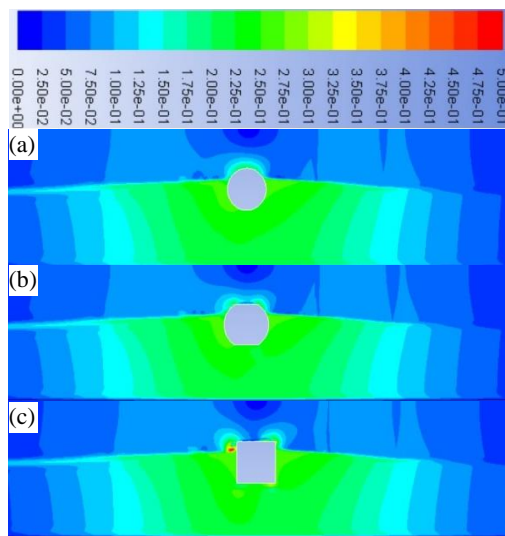


Fig. 15. Velocity contour plot of a SW relating with the floating breakwater for models 1 (a), 2 (b), and 3 (c) for SW height of 0.1 m related with $t=16.2 \text{ s}$.

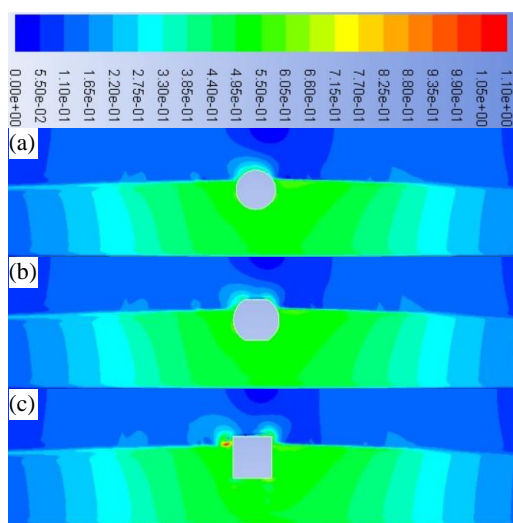


Fig. 16. Velocity contour plot of a SW interacting with the floating breakwater for models 1 (a), 2 (b), and 3 (c) for SW height of 0.2 m related with $t=14.6 \text{ s}$.

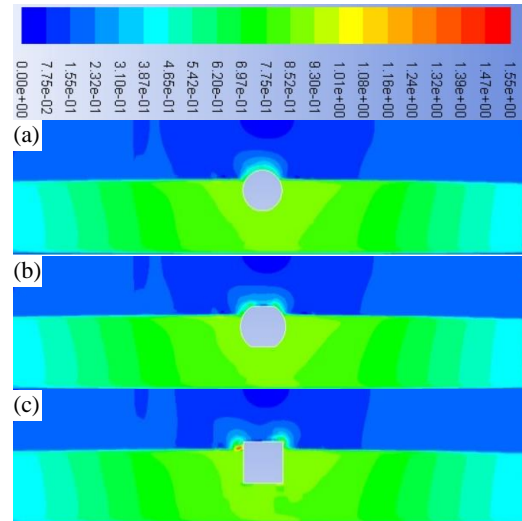


Fig. 17. Velocity contour plot of a SW relating with the floating breakwater for models 1 (a), 2 (b), and 3 (c) for SW height of 0.3 m related with $t=13.6 \text{ s}$.

velocity contour values around square floating breakwaters are greater than other floating breakwaters.

4. CONCLUSION

This study numerically evaluated interaction between SWs of varying heights and floating breakwaters of varying shapes and densities. We defined a 2D NWT for solving the VOF model with the RNG $k-\epsilon$ turbulence one and the dynamic mesh method. We found the numerical work to be capable of capturing the free surface with high accuracy. The floating breakwaters' heave and sway motions, kinetic energies, and horizontal and vertical hydrodynamic forces were calculated for various conditions. Obtained results from the analyses are given as:

- The computational outputs indicate that floating breakwaters' performances significantly depend on their shapes and densities and on the SWs' heights.
- Wave height has a direct impact on floating breakwaters' heave and sway motions.
- For all models, maximum heave and sway motions were obtained at a wave height of 0.3 m.
- In all models, the horizontal and vertical forces increased with the SW heights.
- Maximum horizontal and vertical hydrodynamic forces occurred in Model 1 when the wave height was 0.3 m.
- The floating breakwaters' kinetic energy increased with increasing SW height and breakwater density.
- The kinetic energy of the breakwater in Model 1 at a wave height of 0.3 m and a breakwater density of 900 kg/m^3 was greater than that of the other models.

h. The investigated NWT can reflect the relationship between a SW and a floating breakwater with high accuracy.

ACKNOWLEDGMENT

The third author acknowledges the support provided by NSTDA under the Research Chair Grant, and the Thailand Science Research and Innovation (TSRI) under Fundamental Fund 2022.

REFERENCES

- ANSYS, Inc. ANSYS Fluent Theory Guide (2013). ANSYS, Inc.: Canonsburg, PA, USA. pp. 724–746.
- Batchelor, G. K. (2000). *An Introduction to Fluid Dynamics*. Cambridge University Press: Cambridge, UK.
- Chen, Q., J. Zang, J. Birchall, D. Ning, X. Zhao and J. Gao (2020). On the hydrodynamic performance of a vertical pile-restrained WEC-type floating breakwater. *Renewable Energy* 146, 414-425.
- Cheng, L. and P. Lin (2018). The numerical modeling of coupled motions of a moored floating body in waves. *Water* 10, 1748.
- Eren, E. T., M. Tabatabaei-malazi and G. Temir (2020). Numerical investigation on the collision between a solitary wave and a moving cylinder. *Water* 12, 2167.
- Hu, X., Y. Jiang and D. Cai (2017). Numerical modeling and simulation of wave impact of a circular cylinder during the submergence process. *Modelling and Simulation in Engineering* 1–14.
- Ito, S. (1977). *Study of the transient heave oscillation of a floating cylinder*. Gr. thesis, Massachusetts Institute of Technology, Cambridge, USA.
- Ji, C., Y. Cheng, K. Yang and G. Oleg (2017). Numerical and experimental investigation of hydrodynamic performance of a cylindrical dual pontoon-net floating breakwater. *Coastal Engineering* 129, 1–16.
- Liang, D., W. Jian, S. Shao, R. Chen and K. Yung (2017). Incompressible SPH simulation of solitary wave interaction with movable seawalls. *Journal of Fluids and Structures* 69, 72-88.
- Lin, P. (2006) A multiple-layer r-coordinate model for simulation. *Computers & Fluids* 35, 147–167.
- Lin, P. (2007). A fixed-grid model for simulation of a moving body in free surface flows. *Computers & Fluids* 36, 549–561.
- Liu, X., P. Lin and S. Shao (2014). An ISPH simulation of coupled structure interaction with free surface flows. *Journal of Fluids and Structures* 48, 46-61.
- Liu, Z. and Y. Wang (2020a). Studies of submerged moored box-type floating breakwaters with different shapes of cross-sections using SPH. *Coastal Engineering* 158, 103687.
- Liu, Z. and Y. Wang (2020b). Numerical investigations and optimizations of typical submerged box-type floating breakwaters using SPH. *Ocean Engineering* 209, 107475.
- Maskell, S. J. and F. Ursell (1970). The transient motion of a floating body. *Journal of Fluid Mechanics* 44, 303-13.
- Nikpoura, A. H. and M. N. Moghima and M. A. Badrib (2019). Experimental study of wave attenuation in trapezoidal floating breakwaters. *China Ocean Engineering* 33(1), 103–113.
- Ninga, D. Z. X. L. Zhaoa, M. Zhaoa, M. Hannc and H. G. Kang (2017). Analytical investigation of hydrodynamic performance of a dual pontoon WEC-type breakwater. *Applied Ocean Research* 65, 102–111.
- Olcay, A. B. and M. Tabatabaei Malazi (2016). The effects of a longfin inshore squid's fins on propulsive efficiency during underwater swimming. *Ocean Engineering* 128, 173–182.
- Peng, W., W. Lee, S. H. Shin and N. Mizutani (2013). Numerical simulation of interactions between water waves and inclined-moored submerged floating breakwaters. *Coastal Engineering* 82, 76–87.
- Qu, K., W. Y. Sun, S. Kraatz. B. Deng and C. B. Jiang (2017). Effects of floating breakwater on hydrodynamic load of low-lying bridge deck under impact of cnoidal wave. *Ocean Engineering* 203, 107217.
- Ren, Y., M. Luo and P. Lin (2019). Consistent Particle Method Simulation of Solitary Wave Interaction with a Submerged Breakwater. *Water* 11, 261.
- Seiffert, B., M. Hayatdavoodi and R. C. Ertekin (2014). Experiments and computations of solitary-wave forces on a coastal-bridge deck. Part I: Flat Plate. *Coastal Engineering* 88, 194–209.
- Shen, Y. M. C. O. Ng and Y. H. Zheng (2004). Simulation of wave propagation over a submerged bar using the VOF method with a two-equation k- ϵ turbulence modeling. *Ocean Engineering* 31, 87–95.
- Tabatabaei Malazi, M., E. T. Eren, J. Luo, S. Mi and G. Temir (2020). Three-Dimensional Fluid–Structure Interaction case study on elastic beam. *Journal of Marine Science and Engineering* 8, 714.
- Tian, X., Q. Wang, G., Liu, W. Deng and Z. Gao (2018). Numerical and Experimental Studies on a Three-Dimensional Numerical Wave Tank. *Institute of Electrical and Electronics Engineers Access* 6, 6585–6593.
- Tsai, C. P., Y. C. Chen, C. J. Chen and C. Lin (2016).

- Simulation of the effect of breakwater on the propagation of solitary waves. *Journal of Marine Science and Technology* 24 (4), 780–789.
- Vasudev, K. L., R. Sharma and S. K. Bhattacharyya (2014). A multi-objective optimization design framework integrated with CFD for the design of AUVs. *Methods in Oceanography* 10, 138–165.
- Wu, N. J., S. H. Hsiao, H. H., Chen and R. Y. Yang (2016). The study on solitary waves generated by a piston-type wave maker. *Ocean Engineering* 117, 114–129.
- You, R., G. He, J. Wang and P. Liu (2019). CIP-based analysis on strongly nonlinear interaction between solitary waves and submerged flat plate. *Ocean Engineering* 176, 211–221.
- Yu, P., G. Chen, X. Peng, Y. Zhang, H. Zhang and W. Wang (2021). Verification and application of 2-D DDA-SPH method in solving fluid–structure interaction problems. *Journal of Fluids and Structures* 102, 103252.
- Zhan, J. M., X. B. Chen, Y. J. Gong and W. Q. Hu (2017). Numerical investigation of the interaction between an inverse T-type fixed/floating breakwater and regular/irregular waves. *Ocean Engineering* 137, 110–119.
- Zhang, X., Q. Zeng, and Z. Liu (2019). Hydrodynamic performance of rectangular heaving buoys for an integrated floating breakwater. *Journal of Marine Science and Engineering* 7, 239.
- Zheng, X., X. Lv, Q. Ma, W. Duan, A. Khayyer and S. Shao (2018). An improved solid boundary treatment for wave–float interactions using ISPH method. *International Journal of Naval Architecture and Ocean Engineering* 10, 329–347.